Layer-dependent reactivity in the Fe/Mo(110) epitaxial ultrathin film system

S. Murphy,* G. Mariotto, N. Berdunov, and I. V. Shvets
SFI Laboratory, Physics Department, Trinity College, Dublin 2, Ireland
(Received 29 May 2003; published 29 October 2003)

Fe films in the $0.4 \leqslant \theta \leqslant 4.7$ ML (monolayer) coverage range were deposited on a Mo(110) substrate at temperatures between 300 K and 700 K, under ultrahigh vacuum conditions. The adsorption of CO, CO_2, H_2O, and O_2 onto these films from the residual gas within the Ultrahigh vacuum system has been studied using scanning tunneling microscopy, low-energy electron diffraction, and Auger electron spectroscopy analysis. The first, second, and third Fe layers display distinct structures, correlated to the different adsorption characteristics of each layer. Separate mechanisms are identified as the cause of this layer-dependent reactivity. The difference between the first and second Fe layers is attributed to the difference in charge polarization effected between these layers and the substrate. However, our results prove that the different adsorption characteristics of the pseudomorphically strained first layer and the two-dimensionally strain-relieved third layer are directly linked to the film strain.

DOI: 10.1103/PhysRevB.68.165419 PACS number(s): 68.55.Ac, 68.55.Jk

I. INTRODUCTION

The structural and electronic properties of heteroepitaxial ultrathin film systems have been actively investigated in recent years because of their chemical properties. These heterogeneous systems often display enhanced catalytic properties, compared to the surfaces of their constituent metals.[1,2] The binding of simple probe molecules such as CO, H_2, or O_2 can be increased or decreased, depending on the nature of the bimetallic bond between the film and substrate,[3,4] the film strain introduced by lattice mismatch at the interface,[5,6] and the influence of the film morphology on the availability of binding sites.[7] In each case, the resulting adsorption characteristics of the film surface can depend on the film thickness. While the influence of electronic coupling between the film and substrate may be localized to the first few layers of the film, the influence of film strain and film morphology can be present over many layers.

In this study, we report on the layer-dependent reactivity to residual gas adsorption for ultrathin Fe films grown on a Mo(110) surface. The Fe/Mo(110) system is an interesting bimetallic system to investigate, as the lattice mismatch between the film and substrate produces a large tensile strain in the pseudomorphic film $[(a_{\mathrm{Mo}}-a_{\mathrm{Fe}})/a_{\mathrm{Fe}}=9.8\%]$. In addition, a wide variety of nanostructures may be grown by controlling the substrate temperature, deposition rate, and substrate step density and orientation. The growth of this system has been investigated by a range of experimental techniques[8–13] and has displayed many similarities to the more widely studied Fe/W(110) system.[14–22] Layer-dependent reactivity has previously been observed in the Fe/W(110) system, for films consisting of alternating monolayer- and double-layer stripes.[18] A regular (2×2) structure was atomically resolved by scanning tunneling microscopy (STM) on double-layer Fe stripes grown at elevated temperatures, while an irregular (2×2) structure was observed on the monolayer stripes.[23] These structures were attributed to CO adsorption from the residual gas and were routinely used to distinguish the monolayer- and double-layer components in the STM images.

The growth of Fe films on Mo(110) may be summarized as follows. At room temperature, films grow layer by layer for the first and second Fe layers. The first layer grows in pseudomorphic registry with the substrate despite the large tensile strain. Randomly spaced dislocation lines are formed in the second Fe layer along the $[00\bar{1}]$ crystallographic direction, which partially relieves the tensile strain in the second layer along the orthogonal $[1\bar{1}0]$ direction. A transition from layer by layer to Stranski-Krastanov growth occurs in the third layer; the exact coverage at which this transition occurs is determined by the substrate temperature and the deposition rate. A two-dimensional dislocation network is formed in the third-layer islands, which relieves the strain along both the $[00\bar{1}]$ and $[1\bar{1}0]$ directions. At elevated substrate temperatures, a pseudomorphic first Fe layer is formed on the surface through the step-flow growth mechanism. Depending on the step orientation on the surface,[22] submonolayer coverages of Fe can decorate the substrate steps as an array of continuous monolayer thick stripes. The growth of the second Fe layer follows a similar pattern, resulting in the formation of arrays of alternating single- and double-layer stripes.[21] Dislocation lines are formed in the double-layer stripes along the $[00\bar{1}]$ direction, analgous to the growth around 300 K. For thicker films, distinctive wedge-shaped islands are formed on the surface.[10–12] These islands cross several substrate terraces while maintaining a flat (110) surface that is unbroken by steps. The substrate between these islands is covered by a closed pseudomorphic Fe layer. A two-dimensional dislocation network is formed in the fourth layer of the wedge-shaped islands, originating from an array of regularly spaced dislocation lines in the third layer.[13]

One further issue that excites interest in this system is that the various Fe nanostructures that can be grown on W(110) possess a variety of novel magnetic properties.[14,16–22] The adsorption of species from the residual gas has significant implications for the magnetic properties of these films. For

example, an adsorption-driven spin reorientation transition is observed in double-layer Fe stripes grown on stepped W(110) surfaces, through exposure to the residual gas within the ultrahigh vacuum system[24] or through controlled dosing of the surface with CO, O_2, or H_2.[25] This may also be true of the very similar nanostructures that are formed in the Fe/Mo(110) system, though the magnetic properties of this system have not been widely investigated.

II. EXPERIMENT

The sample preparation and analysis were performed in an ultrahigh vacuum (UHV) system with a base pressure in the low 10^{-10} torr. The three-chamber system comprised two chambers equipped with room- and low-temperature scanning tunneling microscopes, respectively and a third chamber equipped with an *e*-beam evaporator, resistive and *e*-beam substrate heaters, and an ion source. The system was also equipped with four-grid reverse-view optics for low-energy electron diffraction (LEED) and a cylindrical mirror analyzer for Auger electron spectroscopy (AES). A quadrupole mass spectrometer (mks instruments) with a 1–100 amu mass range was used to monitor the residual gas composition in the UHV system. Typical partial pressures of 4×10^{-11} torr for H_2O, 3×10^{-11} torr for CO, 7×10^{-12} torr for CO_2, and 3×10^{-13} torr for O_2 were measured in the deposition chamber, while H_2 made up most of the remainder.

The substrate was prepared from a 4N purity Mo single crystal, miscut by $0.7\pm0.2°$ from the (110) crystal plane to produce a surface with steps oriented along the $[1\bar{1}1]$ direction and an average terrace width of around 200 Å. The surface was cleaned by annealing at $1300\leqslant T\leqslant1550$ K in an O_2 partial pressure of 5×10^{-7} torr in cycles of 30–60 min. After each oxidation cycle, the substrate was flash annealed several times by electron-bombardment to 2400 K for 10–15 s intervals under UHV conditions. After this preparation, no impurities were detected on the surface by AES, while a sharp (1×1) LEED pattern consistent with the unreconstructed Mo(110) surface was obtained. The sample was further cleaned by flash annealing several times to 2400 K, 30-40 min prior to each evaporation. AES analysis of the clean Mo(110) surface indicated that the surface did not become contaminated by either adsorption from the residual gas or diffusion from the bulk for periods of up to 6 h at room temperature or for up to 1.75 h when annealed at 690 K. The films were deposited on the clean surface by electron-beam evaporation of a 3N purity Fe rod. This rod was outgassed for several hours before its first use and was then outgassed for a further 1-2 h prior to each subsequent evaporation. The evaporator was enclosed in a liquid-nitrogen cooled insert, so that the chamber pressure typically remained below 2×10^{-10} torr during deposition. The deposition flux was monitored by a quartz crystal balance, while the substrate temperature was measured by a thermocouple attached to the sample stage. The Fe film coverage θ is described in terms of pseudomorphic monolayers (ML), where the packing density of a pseudomorphic monolayer is equal to that of the Mo(110) surface ($\sim1.43\times10^{19}$ atoms m^{-2}).

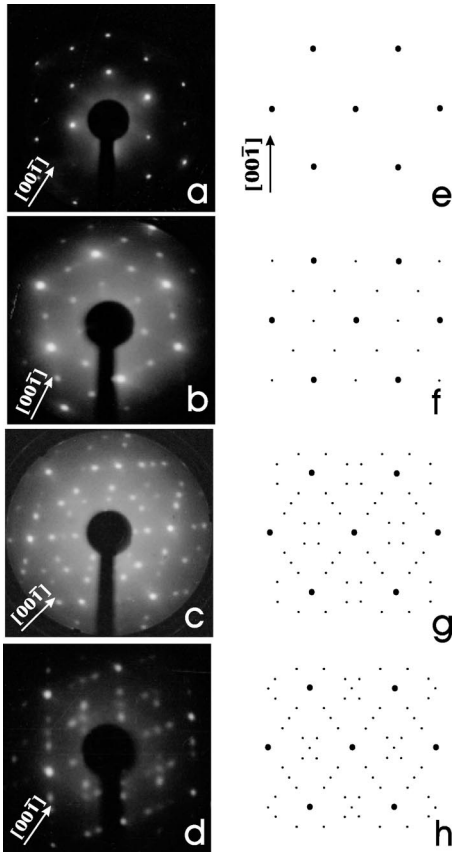

FIG. 1. (a) (1×1) LEED pattern of the clean unreconstructed Mo(110) surface; beam energy $E=226$ eV. (b) $p(2\times2)$ pattern from a 0.95 ML Fe film grown at 300 ± 15 K, within 1–5 h of exposure to the residual gas; $E=123$ eV. (c) $p(3\times2)$ pattern typically obtained on films after 5–25 h exposure; $E=103$ eV. (d) $p(3\times2)$ and $p(2\times2)$ domains observed during $p(2\times2)\rightarrow p(3\times2)$ transition on a 1.8 ML film grown at 340 ± 15 K, after ~15 h of exposure; $E=98$ eV. (e)–(h) The corresponding schematic representations of the LEED patterns shown in (a)–(d).

III. RESULTS AND DISCUSSION

Figure 1 shows the LEED patterns acquired from the clean Mo(110) surface and a series of films from 0.95 ML to 1.8 ML coverage, which were deposited at temperatures between 300 K and 345 K. In the $0.4\leqslant\theta\leqslant1.8$ ML coverage range, freshly deposited films gave a (1×1) LEED pattern similar to that observed for the clean Mo(110) surface, shown in Fig. 1(a). However, within ~1–5 h of exposure to the residual gas within the UHV system, a LEED pattern similar to that shown in Fig. 1(b) was obtained. The pattern is identified as a $p(2\times2)$ structure with respect to the primitive unit cell of the surface. A similar LEED pattern is commonly observed on the Fe(110) surface, upon the adsorption of 0.25 ML of O_2.[26,27] In this case, the pattern is identified as a $c(2\times2)$ reconstruction, with respect to the nonprimitive unit cell of the surface.

With further exposure to the residual gas a $p(3\times2)$ structure like that shown in Fig. 1(c) was formed on the surface. This pattern typically appeared on films between 5 and 25 h after deposition. The exposure time required to produce this

$p(2\times2)\rightarrow p(3\times2)$ transition varied between different films due to subtle differences in coverage, morphology, strain, etc. The pattern shown in Fig. 1(c) was obtained on a 1.8 ML Fe film grown at 340 ± 15 K after ~8 h of exposure. In some cases, both the $p(2\times2)$ and the $p(3\times2)$ structures could be observed simultaneously during the $p(2\times2)\rightarrow p(3\times2)$ transition. An example is presented in Fig. 1(d), which shows the LEED pattern obtained on a 1.8 ML Fe film grown at 340 ± 15 K, after ~15 h exposure to the residual gas within the UHV system. This pattern is a superposition of the $p(2\times2)$ and $p(3\times2)$ patterns shown in Figs. 1(f) and 1(g) respectively.

Analysis by AES indicated that the onset of the $p(2\times2)$ LEED pattern corresponded to the appearance of carbon and oxygen on the films. The concentrations of these contaminants were found to increase with continued exposure to the residual gas within the UHV system, leading to the onset of the $p(3\times2)$ pattern. The carbon concentration on the surface was generally found to be higher and to increase more rapidly than the oxygen concentration. These contaminants most likely originated from H_2O, O_2, CO, and CO_2 in the residual gas. The dominant presence of these gases in the system was confirmed using a quadrupole mass spectrometer.

Figure 2 shows a series of STM images of a 1.6 ML Fe film grown on Mo(110) at 330 ± 15 K. A $p(2\times2)$ LEED pattern was obtained on this film; the STM images were taken ~11 h after film deposition. The substrate step edges are aligned parallel to the $[1\bar{1}1]$ crystallographic direction. The first Fe layer is completely closed and the remaining Fe either decorates the step edges or forms two-dimensional islands on top of the first layer terraces. LEED analysis of submonolayer coverage films has indicated that the first Fe layer is pseudomorphically strained on top of the Mo(110) surface, despite the large lattice mismatch. However, strain-relieving dislocation lines can be seen in some of the larger second-layer Fe islands in Fig. 2(a). These dislocations can form favorable nucleation sites for third-layer islands.[13] The higher-resolution images of the film, shown in Figs. 2(b–f), highlight the markedly different atomic structure formed on top of the first and second Fe layers after exposure to the residual gas.

An ordered $p(2\times2)$ structure is atomically resolved on top of the second Fe layer, as shown in Fig. 2(d). This structure is resolved in more detail in Fig. 2(e), where the conventional unit cell of the $p(2\times2)$ superlattice is indicated. The dimensions of this centered-rectangular cell were measured to be 9.4 ± 0.2 Å and 5.7 ± 0.2 Å along the $[1\bar{1}0]$ and $[001]$ directions, respectively, while the corrugation amplitude of the structure was measured to be 0.3 ± 0.1 Å along these directions. An antiphase domain boundary between two adjacent $p(2\times2)$ domains is also apparent in Fig. 2(e). At the antiphase domain boundary, there is a shift of half a lattice spacing between the domains, when viewed along the $[1\bar{1}1]$ direction.

As mentioned earlier, a (2×2) structure very similar to this, has been atomically resolved by STM at room temperature on double-layer Fe stripes grown on W(110), where it was attributed to the adsorption of CO from the residual

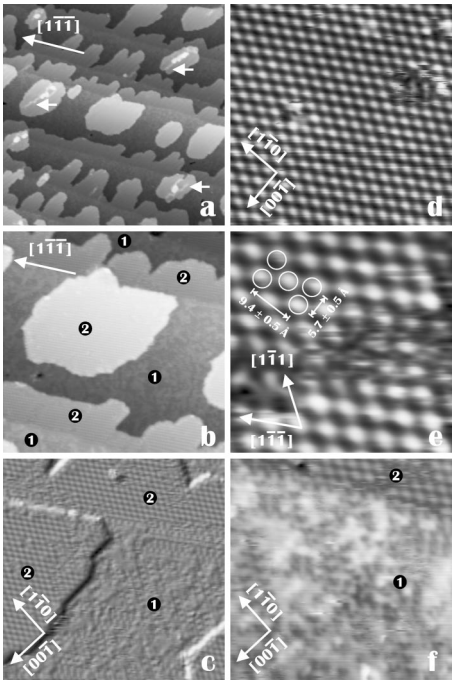

FIG. 2. (a) 1000×1000 Å^2 STM image of a 1.6-ML Fe film grown on Mo(110) at 330 ± 15 K. Arrows indicate the positions of misfit dislocations in second-layer Fe islands. (b) 400×400 Å^2 image with the local film thickness indicated in Fe monolayers. (c) 190×190 Å^2 derivate image highlighting the different structures produced on the first and second Fe layers. Patches of $p(2\times2)$ on the first Fe layer are highlighted by white rectangles. (d) 91×91 Å^2 image of the ordered $p(2\times2)$ structure formed on the second Fe layer by the adsorption of oxygen. (e) 45×45 Å^2 image showing the nonprimitive unit cell of the ordered $p(2\times2)$ superlattice. (f) 91×91 Å^2 image of the disordered $p(2\times2)$ structure formed on the first Fe layer by the dissociative adsorption of CO, CO_2, and oxygen.

gas.[23] Molecular dissociation of CO has been found to occur on a monolayer Fe film on W(110) at temperatures between 300 and 350 K.[28] The STM images shown in Figs. 2(d) and 2(e) indicate that the $p(2\times2)$ structure is formed by a single atomic species. One might expect that if the structure was formed by molecularly adsorbed CO, the STM tip would cause some perturbation as it moved across the surface, which was not observed to be the case. The structure shown in Figs. 2(d) and 2(e) is attributed to the adsorption of oxygen atoms on top of the second Fe layer. The LEED pattern produced by the surface shown in Fig. 2 is identical to that produced by the $c(2\times2)$ oxygen reconstructed Fe(110) surface.[26,27] Atomically resolved STM data of that surface have also revealed a structure which is almost identical to that shown in Fig. 2(d), including antiphase domain boundaries like the one shown in Fig. 2(e).[29,30] To confirm this, a freshly deposited 1.2 ML film displaying a (1×1) LEED pattern was exposed to a partial pressure of 5×10^{-9} torr of 4.8N purity O_2 for 1 min. This corresponds to an exposure of 0.3 L where $1\ \mathrm{L}=10^{-6}$ torr s. It was found that after this exposure, the film displayed a $p(2\times2)$ LEED pattern like that shown in Fig. 1(b). A schematic representation of the oxygen adsorption structure is presented in Fig. 3(a), the

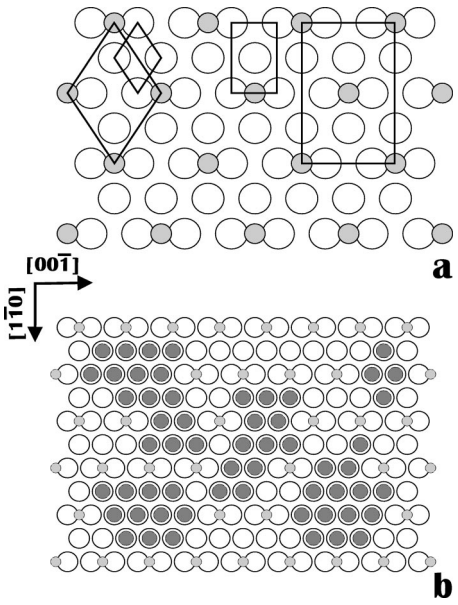

FIG. 3. (a) Schematic representation of the oxygen-induced reconstruction found on the second Fe layer on Mo(110). Large open circles represent Fe atoms and the smaller shaded circles represent oxygen atoms. The primitive unit cell of the surface is marked on the left of the image (small tetragon); the reconstruction may be identified as $p(2\times2)$ with respect to the primitive cell (large tetragon). The non-primitive unit cell of the surface is marked on the right of the image (small rectangle); the reconstruction may be identified as $c(2\times2)$ with respect to the nonprimitive cell (large rectangle). (b) Model of the structure found on the pseudomorphically strained first Fe layer on Mo(110). Dark circles represent carbon atoms. The carbon atoms aggregate into clusters, while the oxygen atoms are arranged in a $p(2\times2)$ structure between these clusters.

positioning of the oxygen atoms in the twofold long bridge sites of the surface is based on the results of electron energy loss spectroscopy (EELS) studies.[31]

It was already stated that AES analysis of these films indicated that both carbon and oxygen were present on the surface. Since the second Fe layer is covered by oxygen alone, then the dissociated carbon must cover the first Fe layer. This is supported by the STM evidence presented in Fig. 2(f), which shows an atomically resolved STM image of the first Fe layer of the 1.6 ML film. In comparison to the ordered structure found on top of the second Fe layer, the structure on the first Fe layer does not display any long-range order in the STM data. However, there are some patches of short-range order [highlighted in Fig. 2(c)], which were identified as a $p(2\times2)$ structure. A $p(2\times2)$ LEED pattern was also observed by us on submonolayer coverage films, where each film consisted of a partially closed pseudomorphic monolayer. This confirmed that the $p(2\times2)$ reconstruction was also present on the first Fe layer of the film. In Fig. 2(f), it is clear that more than one species (i.e., carbon and oxygen) is adsorbed on top of the first Fe layer. The corrugation amplitude measured by STM on the first Fe layer was approximately twice that found on the second Fe layer. Figure 2(f) suggests that the carbon atoms aggregate into clusters, while the oxygen atoms are arranged in a $p(2\times2)$ structure in the patches between these clusters. A simple model of this structure is presented in Fig. 3(b). The positioning of the carbon atoms in on-top sites is chosen for simplicity, however, it appears that the carbon atoms can occupy several possible bonding sites, which would explain the AES observation that the carbon concentration on the films was generally higher and increased faster than the oxygen concentration.

For the 1.6-ML film shown in Fig. 2 we estimate that $\sim$80% of the first Fe layer is covered with carbon, which corresponds to 32% of the exposed surface area. Assuming that the carbon lies in one-to-one registry with the underlying iron atoms we calculate an atomic packing density of 4.6×10^{18} atoms m^{-2} for carbon. The oxygen induced $p(2\times2)$ structure, which corresponds to a coverage of 0.25 ML, covers the remaining exposed surface area so that we calculate a packing density of 2.4×10^{18} atoms m^{-2} for oxygen. The O/C ratio estimated from the STM data is therefore 0.52, which is close to the value of 0.58 determined from AES measurements taken on the surface after the STM session. This clearly demonstrates that all of the carbon and oxygen atoms are adsorbed two dimensionally on the surface of the film.

In Fig. 2, the second-layer Fe that decorates the surface step edges can be readily distinguished by the presence of a fractional step, from the first Fe layer that covers the substrate terraces. This is clearly illustrated in Fig. 4, which shows a high-resolution image of a surface step; the local film thickness changes from 1 to 2 ML as the film crosses the step. The line profile in Fig. 4(b) was taken across the step in Fig. 4(a) along the [001] direction; a fractional step of 0.3 ± 0.1 Å height is apparent between the first and second Fe layers. A similar effect has been observed by STM on clean Fe films deposited on the W(110) surface.[14,17,25] This fractional step is either due to a difference in the local density of states or is the result of pseudomorphically fitting the smaller Fe atoms (atom radius 140 pm) on top of the larger Mo atoms (atom radius 145 pm), as shown schematically in Fig. 4(c).

Figure 5 shows a series of STM images taken on a 1.8 ML Fe film grown on Mo(110) at 340 ± 15 K. The LEED pattern obtained on this surface is shown in Fig. 1(d); domains of both $p(2\times2)$ and $p(3\times2)$ reconstructions are found on the surface. AES analysis has indicated that the transition between the $p(2\times2)$ and $p(3\times2)$ structures corresponds to a large increase in the carbon concentration on the surface, while the oxygen concentration rises only slightly. From Fig. 5, it is clear that the $p(2\times2)$ structure remains largely intact on the second Fe layer, while the $p(3\times2)$ structure is formed on the first Fe layer. In Figs. 5(a) and 5(c), it can be seen that the $p(2\times2)$ structure on the second Fe layer is broken up in some areas. This may be the initial stage of the transformation of the second layer structure into the $p(3\times2)$ phase, which would eventually lead to the LEED pattern shown in Fig. 1(c). This suggests that the $p(2\times2)\rightarrow p(3\times2)$ transition begins on the second layer only after it has been completed on the first layer.

Figure 5(d) shows a 190×190 Å^2 image of a second Fe layer island with dislocation lines running along the [001]

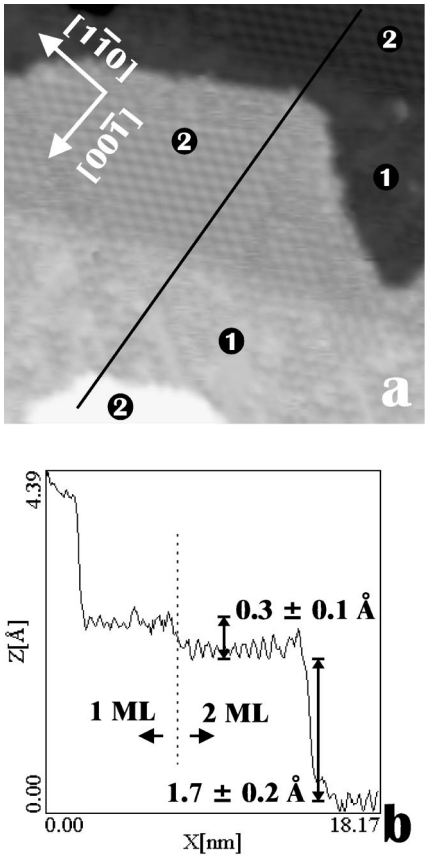

FIG. 4. (a) 150×150 Å^2 image showing the transition in local film thickness from 1 to 2 ML at a surface step. The local film thickness in monolayers is indicated. The black line along the [001] direction denotes the line profile shown in (b). The height of the fractional step between the first and second Fe layers is 0.3 ±0.1 Å, while an overall step height of 2.0±0.3 Å was measured. (c) A simplified ball model that shows how the smaller atomic radius of the Fe atoms compared to the Mo atoms may lead to the fractional step between the first and second Fe layers at a substrate step.

direction. The presence of these strain-relieving dislocations does not appear to have any effect on the $p(2\times2)$ structure also present on the island. However, the formation of a two-dimensional network of dislocations in the third Fe layer, as shown in Fig. 6(a), inhibits the formation of the $p(2\times2)$ structure. Figure 6 shows the STM and LEED data for a 2.4 ML Fe film grown on Mo(110) at 325±15 K. The LEED pattern obtained from this film, shown in Fig. 6(b), displays

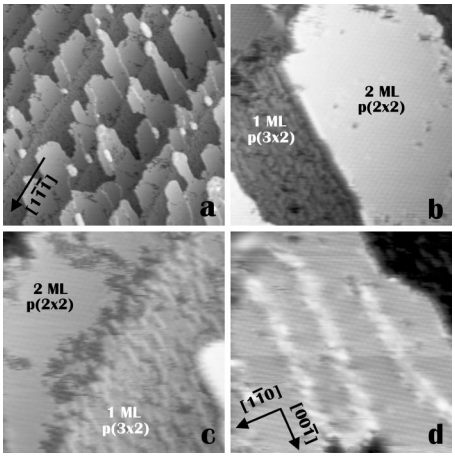

FIG. 5. (a) 1000×1000 Å^2 image of a 1.8 ML Fe film grown at 340±15 K. (b) 230×230 Å^2 and (c) 190×190 Å^2 images of the same film showing the different structures on the first and second Fe layers. (d) 190×190 Å^2 image of a large second layer Fe island containing dislocation lines that propagate along the [001] direction.

satellite spots around the integral-order reflections, which are produced by lattice distortions within the film arising from the dislocation network. The LEED pattern does not display any half-order spots that would be consistent with a $p(2\times2)$ structure. This is supported by the STM data in Figs. 6(c) and 6(d), which clearly show that the $p(2\times2)$ structure disappears where the dislocation network is formed. How-

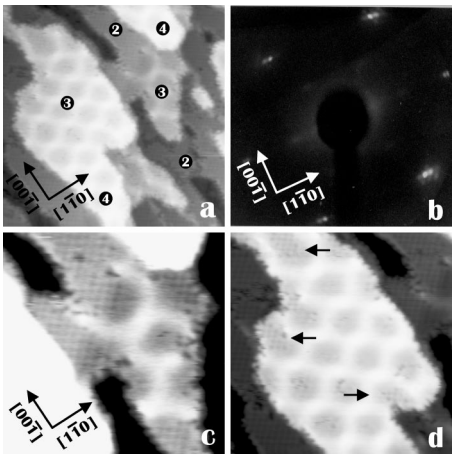

FIG. 6. (a) 300×300 Å^2 image of a 2.4 ML Fe film grown at 325±15 K, showing the two-dimensional dislocation network formed in the third Fe layer of the film. The local island thickness in Fe monolayers is indicated. (b) The LEED pattern formed by this film at a primary beam energy of $E_{beam}=71$ eV. The satellite spots around the integral-order reflections are due to lattice distortions produced in the film by the dislocation network. (c) 140×140 Å^2 contrast-enhanced zoom-in of the onset of the dislocation network where the local film thickness increases from two to three Fe layers. (d) 190×190 Å^2 image of a third-layer Fe island—the arrows mark regions where a $p(2\times2)$ structure can still be observed. These areas correspond to the locations where the dislocation network is disrupted.

ever, the $p(2\times2)$ structure does persist in patches at the edges of Fe islands where the dislocation network is disrupted. As these areas where the dislocation network is disrupted represent only a small fraction of the overall surface, the $p(2\times2)$ reflections from such areas are not noticeable in the LEED pattern of the surface. Preliminary AES results show that the carbon and oxygen adsorption on different coverage films as a function of exposure time is lower for both species on the thicker Fe films which have lower strain, though this needs to be studied in more detail using controlled dosing with single-gas species.

The fact that the $p(2\times2)$ structure is absent on Fe layers that are not pseudomorphically strained appears at first to be in conflict with the observation of this structure on the bulk surface. The average effect of the two-dimensional dislocation network shown in Fig. 6 is to lower the overall tensile strain in the Fe layer, by increasing the atomic packing density through the introduction of additional Fe atoms at the dislocations. However, it is also clear from Fig. 6 that the strain in the Fe layer is locally modulated by the network, between regions of compressive strain at the dislocations (due to the insertion of extra Fe atoms) and regions of tensile strain in the areas between the dislocations. This localized modulation of the strain in the Fe layer is the critical factor that prevents the formation of a long-range ordered $p(2\times2)$ structure as appears on the second Fe layer, which for the most part is uniformly strained. With increasing film thickness, the relaxation of the film lattice converges towards the unstrained state found in the bulk and the dislocation network disappears from the surface. As a result, the reappearance of the $p(2\times2)$ structure can then be expected.

There is a clear correlation between the abrupt changes in the film strain between the first and third Fe layers and the different adsorption characteristics of each layer. The lattice mismatch in the Fe/Mo(110) epitaxial system produces a large tensile strain ($\sim10\%$) in the first Fe layer, which is in pseudomorphic registry with the Mo(110) surface. It has been shown that tensile strain induces a narrowing in the energy of the *d*-band states within the strained Fe layer and a shift in the center of the *d* band to higher energies, resulting in enhanced binding energies of adsorbed molecules.[32] As a result, both carbon and oxygen can be found on the first Fe layer. The strain relief is much greater in the third layer of the film with the introduction of the two-dimensional dislocation network, which relieves the tensile strain along both the [001] and [110] directions. As a result, neither carbon- nor oxygen-induced structures are observed above this layer.

However, the tensile strain is only partially relieved in the second Fe layer by the introduction of the randomly distributed dislocations that propagate along the [001] direction. These dislocations provide a mostly uniaxial strain relief in this layer along the orthogonal [110] direction. The atomically resolved STM image in Fig. 5(d) clearly shows that the oxygen-induced $p(2\times2)$ structure is unaffected by the presence of these dislocations. It is unlikely that the absence of carbon atoms on the second Fe layer is due to the partial strain relief caused by these dislocations, especially as they are so randomly distributed. The difference between these layers is more likely attributed to the different charge polarization between the first and second layers and the substrate.[3,4] It has been demonstrated experimentally by Auger electron spectroscopy that the charge transfer between an Fe film and a Mo(110) substrate decreases significantly over the coverage range $0\leqslant\theta\leqslant2.0$ ML.[33]

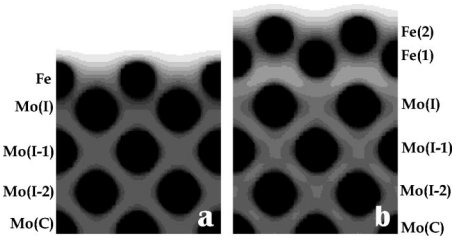

FIG. 7. Calculated charge-density contour maps for (a) one pseudomorphic Fe layer and (b) two pseudomorphic Fe layers on a bulk Mo(110) slab. The contours shown range from zero in the vacuum region to 0.57 $e/\text{Å}^3$ in increments of 3.5×10^{-2} $e/\text{Å}^3$. Mo(C) and Mo(I) denote the substrate layers at the center of the slab and at the film interface, respectively.

To investigate the charge polarization between the film and substrate in the first and second Fe layers, we performed density-functional theory calculations using the plane-wave approximation method. The system was simulated by a seven-layer bulk Mo(110) slab covered on both sides by either a 1 ML or a 2 ML pseudomorphic Fe film. The in-plane lattice parameter in each film was taken to be that of bulk Mo(110) and the interlayer separations were optimized by total-energy calculations. Figures 7(a) and 7(b) show charge-density contour maps for the case of 1 ML Fe and 2 ML Fe, respectively. Comparing the charge densities in the interfacial regions in Figs. 7(a) and 7(b), it is clear that the charge sharing between the first Fe layer and the substrate is reduced when the second Fe layer is added. In addition, in Fig. 7(b) the charge density in the region between layers Fe(2) and Mo(I) is much lower than that between layers Fe(1) and Mo(I-1), indicating that the electronic interaction between the second Fe layer and the substrate is much lower than that experienced by the first Fe layer. These differences in the electronic interaction between the first and second Fe layers and the substrate are reflected in the experimentally observed differences in the adsorption characteristics between these layers.

Figures 8 and 9 show the morphology of two Fe films grown at elevated temperatures; a 1.2 ML film grown at 495 ± 15 K and a 2.4 ML film grown at 515 ± 15 K. At elevated substrate temperatures, the growth of the first and second Fe layers is mediated by the step-flow growth mechanism, where the deposited Fe propagates outwards from a surface step across the underlying terrace. As a result, the surface is characterized by an array of Fe stripes which are oriented parallel to the substrate step direction. These stripes can be 1–2 ML thick, depending on the film coverage. In Fig. 8(a), the first Fe layer is completely closed and LEED analysis has indicated that this layer grows pseudomorphically on top of the Mo substrate. The second Fe layer decorates the surface steps as stripes with an average lateral width of 30–60 Å. There are no dislocation lines in these second-

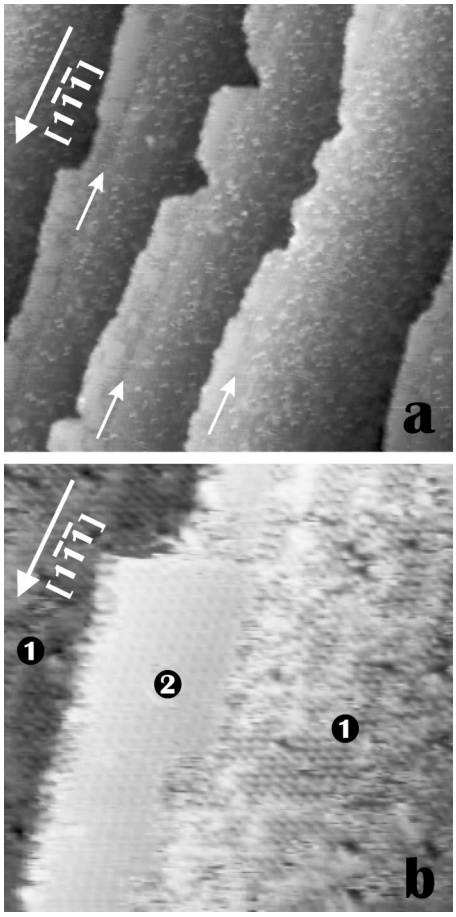

FIG. 8. (a) 594×594 Å^2 image of a 1.2 ML Fe film grown at 495±15 K. The substrate is covered by a closed pseudomorphic monolayer, while the remaining Fe decorates the surface steps. The fractional steps produced at the transition between the first and second Fe layers are highlighted by arrows. (b) 190×190 Å^2 zoom-in of a step, showing the ordered $p(2\times2)$ structure on the second Fe layer and the disordered structure on the first layer.

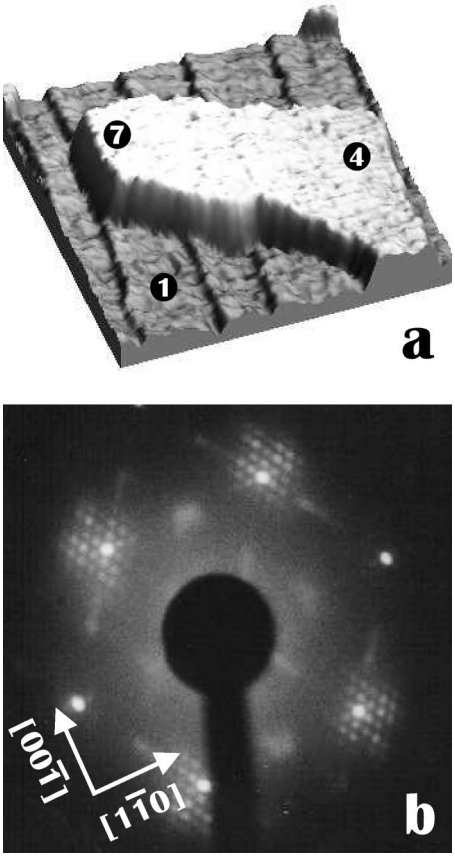

FIG. 9. (a) A three-dimensional perspective of an Fe nanowedge island—the local island thickness varies from four to seven Fe layers, while the substrate is covered by a closed pseudomorphic monolayer. The film is a 2.4 ML nominal coverage Fe film grown at 515±15 K. (b) The LEED pattern produced by the film at a primary beam energy of $E_{beam}=111$ eV. The satellite spots are caused by lattice distortions produced in the islands by the two-dimensional dislocation network, while the half-order spots are produced by the $p(2\times2)$ structure on the strained monolayer between the islands.

layer stripes—the relaxation of atom positions at the outer edge of the stripe is sufficient to relieve the strain in the stripe. However, for stripes with a lateral width in excess of ~100 Å, dislocation lines are formed along the [00$\bar{1}$] direction.

The adsorption behavior of these layers is identical to that observed for films of similar coverage grown at room temperature. In Fig. 8(b), the first layer is covered by a $p(2\times2)$ structure due to the dissociative adsorption of CO, CO_2, and oxygen. No long-range order is observed in the STM images because the carbon atoms form randomly positioned clusters within the $p(2\times2)$ arrangement of oxygen atoms. However, on the second layer an ordered $p(2\times2)$ structure is present due to the adsorption of oxygen alone.

The film morphology changes significantly at higher coverages, where the film is characterized by the formation of distinctive wedge-shaped Fe islands, as illustrated in Fig. 9(a). The mismatch-induced strain in these islands is substantially alleviated by the formation of a two-dimensional dislocation network. A $p(2\times2)$ structure could not be observed by STM on top of these islands. However, the corresponding LEED pattern of this surface, shown in Fig. 9(c), exhibits faint half-order spots, indicating that a $p(2\times2)$ structure is formed on the pseudomorphically strained monolayer that covers the substrate between the islands. This again reflects the tendency of the $p(2\times2)$ structure to form on the uniformly strained Fe layer, while it does not appear on layers where the strain is locally modulated by a dislocation network.

IV. CONCLUSIONS

Fe films in the $0.4\leqslant\theta\leqslant4.7$ ML coverage range were deposited on a Mo(110) substrate at temperatures between 300 K and 700 K. AES analysis has indicated that these films are highly reactive to the adsorption of CO, CO_2, H_2O, and O_2 from the residual gas in the UHV system. STM and LEED analysis of films in the $0.4\leqslant\theta\leqslant2.4$ ML coverage range has indicated that the adsorption characteristics of the first, second, and third Fe layers are very different. These results can be summarized as follows:

(1) CO, CO_2, and oxygen are coadsorbed on the first Fe layer in a structure that does not display any long-range order in the STM images. The carbon atoms aggregate into clusters, while the oxygen atoms are arranged in a $p(2\times2)$ structure.

(2) An ordered $p(2\times2)$ structure is formed on top of the second Fe layer due to the adsorption of a single atomic species. This is identified as oxygen, since exposing a freshly deposited Fe film with 0.3 L of O_2 produces a $(1\times1)\rightarrow p(2\times2)$ transition in the LEED pattern obtained from the surface.

(3) The adsorption of high coverages of CO or CO_2 causes a transition from the $p(2\times2)$ structure to a $p(3\times2)$ reconstruction. This transition begins in the first Fe layer and only occurs in the second layer once the first layer is completely transformed.

(4) The formation of dislocation lines that relieve strain along the $[1\bar{1}0]$ direction does not affect the adsorption characteristics of the film.

(5) The presence of a two-dimensional dislocation network which relieves the mismatch-induced strain in the film along both the $[1\bar{1}0]$ and $[00\bar{1}]$ directions does significantly alter the adsorption characteristics of the film and inhibits the formation of both the $p(2\times2)$ and $p(3\times2)$ structures. The structures are prevented from forming by the local modulation of the layer strain produced by the network, which results in regions of local compressive strain at the dislocations, where extra Fe atoms have been added, and regions of (lowered) tensile strain in the areas between the dislocations.

It can be concluded that the layer-dependent reactivity of the Fe/Mo(110) ultrathin epitaxial film system is the result of distinct film strain and charge polarization effects. The partial strain relief afforded by randomly distributed dislocation lines in the second layer does not significantly affect the adsorption characteristics of this layer when compared to the pseudomorphically strained layer. Rather, the difference in reactivity is more likely the result of the different charge polarization between the first and second layers and the substrate. However, our results prove that the adsorption characteristics are also highly sensitive to the film strain when comparing the pseudomorphically strained first layer and the two-dimensionally strain-relieved third layer. More detailed experiments involving controlled dosing with single-gas species are required to investigate the interaction of O_2, CO_2, CO, etc., with this film system and their effect on the magnetic properties of the Fe films.

ACKNOWLEDGMENTS

This work was supported by the Science Foundation Ireland under Contract No. 00/PI.1/C042 and the 5th Framework Program of the European Commission under project Magnetude Grant No. G5RD-CT-1999-00005.

*Corresponding author. FAX: + 353 1 608 3228; email address: shmurphy@tcd.ie

[1] J.A. Rodriguez, Surf. Sci. Rep. **24**, 223 (1996).
[2] J.H. Larsen and I. Chorkendorff, Surf. Sci. Rep. **35**, 163 (1999).
[3] J.A. Rodriguez, Surf. Sci. **345**, 347 (1996).
[4] Z. Yang and R. Wu, Surf. Sci. **469**, 36 (2000).
[5] E. Kampshoff, E. Hahn, and K. Kern, Phys. Rev. Lett. **73**, 704 (1994).
[6] J. Osing, S. Murphy, and I.V. Shvets, Surf. Sci. **454-456**, 280 (2000).
[7] A. Schlapka, U. Käsberger, D. Menzel, and P. Jakob, Surf. Sci. **502-503**, 129 (2002).
[8] M. Tikhov and E. Bauer, Surf. Sci. **232**, 73 (1990).
[9] B.M. Clemens, R. Osgood, A.P. Payne, B.M. Lairson, S. Brennan, R.L. White, and W.D. Nix, J. Magn. Magn. Mater. **121**, 37 (1993).
[10] J. Malzbender, M. Przybylski, J. Giergiel, and J. Kirschner, Surf. Sci. **414**, 187 (1998).
[11] J. Osing and I.V. Shvets, J. Magn. Magn. Mater. **198-199**, 734 (1999).
[12] J. Osing and I.V. Shvets, Surf. Sci. **433-435**, 440 (1999).
[13] S. Murphy, D. MacMathúna, G. Mariotto, and I.V. Shvets, Phys. Rev. B **66**, 195417 (2002).
[14] H.J. Elmers, J. Hauschild, H. Höche, U. Gradmann, H. Bethge, D. Heuer, and U. Köhler, Phys. Rev. Lett. **73**, 898 (1994).
[15] H. Bethge, D. Heuer, C. Jensen, K. Reshöft, and U. Köhler, Surf. Sci. **331-333**, 878 (1995).
[16] N. Weber, K. Wagner, H.J. Elmers, J. Hauschild, and U. Gradmann, Phys. Rev. B **55**, 14 121 (1997).
[17] J. Hauschild, H. Elmers, and U. Gradmann, Phys. Rev. B **57**, R677 (1998).
[18] H.J. Elmers, J. Hauschild, and U. Gradmann, J. Magn. Magn. Mater. **177-181**, 827 (1998).
[19] D. Sander, A. Enders, C. Schmidthals, D. Reuter, and J. Kirschner, J. Magn. Magn. Mater. **177-181**, 1299 (1998).
[20] D. Sander, A. Enders, C. Schmidthals, D. Reuter, and J. Kirschner, Surf. Sci. **402-404**, 351 (1998).
[21] J. Hauschild, U. Gradmann, and H.J. Elmers, Appl. Phys. Lett. **72**, 3211 (1998).
[22] H.J. Elmers, J. Hauschild, and U. Gradmann, J. Magn. Magn. Mater. **221**, 219 (2000).
[23] H. Elmers, J. Hauschild, and U. Gradmann, Phys. Rev. B **59**, 3688 (1999).
[24] T. Dürkop, H.J. Elmers, and U. Gradmann, J. Magn. Magn. Mater. **172**, L1 (1997).
[25] H.J. Elmers, J. Hauschild, and U. Gradmann, J. Magn. Magn. Mater. **198-199**, 222 (1999).
[26] V.S. Smentkowski and J.T. Yates, Surf. Sci. **232**, 113 (1990).
[27] H.J. Kim and E. Vescovo, Phys. Rev. B **58**, 14 047 (1998).
[28] T.-U. Nahm and R. Gomer, Surf. Sci. **384**, 283 (1997).
[29] A. Wight, N.G. Condon, F.M. Leibsle, G. Worthy, and A. Hodgson, Surf. Sci. **331-333**, 133 (1995).
[30] J. Weissenrieder, M. Göthelid, M. Månsson, H. von Schenck, O. Tjernberg, and U. Karlsson, Surf. Sci. **527**, 163 (2003).
[31] W. Erley and H. Ibach, Solid State Commun. **37**, 937 (1981).
[32] A. Ruban, B. Hammer, P. Stoltze, H.L. Shkriver, and J.K. Nørskov, J. Mol. Catal. A: Chem. **115**, 421 (1997).
[33] T. Magkoev, K. Christmann, P. Lecante, and A. Moutinho, J. Phys.: Condens. Matter **14**, L273 (2002).